

# Direct dark matter search by annual modulation in XMASS-I

K. Abe,<sup>1,5</sup> K. Hiraide,<sup>1,5</sup> K. Ichimura,<sup>1,5</sup> Y. Kishimoto,<sup>1,5</sup> K. Kobayashi,<sup>1,5</sup> M. Kobayashi,<sup>1</sup>  
S. Moriyama,<sup>1,5</sup> M. Nakahata,<sup>1,5</sup> T. Norita,<sup>1</sup> H. Ogawa,<sup>1,5</sup> H. Sekiya,<sup>1,5</sup> O. Takachio,<sup>1</sup> A. Takeda,<sup>1,5</sup>  
M. Yamashita,<sup>1,5</sup> B. S. Yang,<sup>1,5</sup> N. Y. Kim,<sup>2</sup> Y. D. Kim,<sup>2</sup> S. Tasaka,<sup>3</sup> K. Fushimi,<sup>4</sup> J. Liu,<sup>5</sup>  
K. Martens,<sup>5</sup> Y. Suzuki,<sup>5</sup> B. D. Xu,<sup>5</sup> R. Fujita,<sup>7</sup> K. Hosokawa,<sup>7</sup> K. Miuchi,<sup>7</sup> Y. Onishi,<sup>7</sup> N. Oka,<sup>7</sup>  
Y. Takeuchi,<sup>7,5</sup> Y. H. Kim,<sup>8,2</sup> J. S. Lee,<sup>8</sup> K. B. Lee,<sup>8</sup> M. K. Lee,<sup>8</sup> Y. Fukuda,<sup>9</sup> Y. Itow,<sup>10,6</sup>  
R. Kegasa,<sup>10</sup> K. Kobayashi,<sup>10</sup> K. Masuda,<sup>10</sup> H. Takiya,<sup>10</sup> K. Nishijima,<sup>11</sup> and S. Nakamura<sup>12</sup>

(XMASS Collaboration)

<sup>1</sup>*Kamioka Observatory, Institute for Cosmic Ray Research, the University of Tokyo, Higashi-Mozumi, Kamioka, Hida, Gifu, 506-1205, Japan*

<sup>2</sup>*Center of Underground Physics, Institute for Basic Science, 70*

*Yuseong-daero 1689-gil, Yuseong-gu, Daejeon, 305-811, South Korea*

<sup>3</sup>*Information and multimedia center, Gifu University, Gifu 501-1193, Japan*

<sup>4</sup>*Institute of Socio-Arts and Sciences, The University of Tokushima,*

*1-1 Minamijosanjimacho Tokushima city, Tokushima, 770-8502, Japan*

<sup>5</sup>*Kavli Institute for the Physics and Mathematics of the Universe*

*(WPI), the University of Tokyo, Kashiwa, Chiba, 277-8582, Japan*

<sup>6</sup>*Kobayashi-Maskawa Institute for the Origin of Particles and the Universe, Nagoya University, Furo-cho, Chikusa-ku, Nagoya, Aichi, 464-8602, Japan*

<sup>7</sup>*Department of Physics, Kobe University, Kobe, Hyogo 657-8501, Japan*

<sup>8</sup>*Korea Research Institute of Standards and Science, Daejeon 305-340, South Korea*

<sup>9</sup>*Department of Physics, Miyagi University of Education, Sendai, Miyagi 980-0845, Japan*

<sup>10</sup>*Solar Terrestrial Environment Laboratory, Nagoya University, Nagoya, Aichi 464-8602, Japan*

<sup>11</sup>*Department of Physics, Tokai University, Hiratsuka, Kanagawa 259-1292, Japan*

<sup>12</sup>*Department of Physics, Faculty of Engineering, Yokohama National University, Yokohama, Kanagawa 240-8501, Japan*

(Dated: March 23, 2022)

A search for dark matter was conducted with the XMASS detector by means of the expected annual modulation due to the Earth's rotation around the Sun. The data used for this analysis was 359.2 live days  $\times$  832 kg of exposure accumulated between November 2013 and March 2015. The result of a simple modulation analysis, without assuming any specific dark matter model, showed a slight negative amplitude. As the  $p$ -values are 6.1 or 17% in our two independent analyses, these results are consistent with fluctuations. We also set 90% confidence level (C.L.) upper bounds that can be used to test models. When we assume Weakly Interacting Massive Particle (WIMP) dark matter elastically scattering on the target nuclei, we exclude almost all the DAMA/LIBRA allowed region with the modulation analysis. This is the first extensive search probing this region with redan exposure comparable to theirs.

There is strong evidence that about 5 times more dark matter exists in the universe than ordinary matter. Despite its prominence, we do not yet know what dark matter is [1]. Among many candidates for dark matter particles, WIMPs are well motivated and have received the most attention to date. However, no experimental indication for a standard WIMP was found in high sensitivity direct search experiments like LUX [2], XENON100 [3], SuperCDMS [4] for more than a few tens of GeV/ $c^2$  mass. Furthermore the collider experiments did not show any indications of such particles so far. In this situation, low mass WIMPs and other dark matter candidates are gaining more attention. In fact, XMASS, a high light yield and low background detector, probed this possibility looking for signals not only from nuclear recoils but also from electrons emanating from interactions of other candidates such as Axion like particles and Super-WIMPs [5–7]. In the region of light WIMPs, some experiments claim or are interpreted as finding dark matter sig-

nals [8–10], but there is stress among experimental results and this situation has persisted for more than 10 years. The most significant claim is that of the DAMA/LIBRA experiment at the Laboratori Nazionali del Gran Sasso in Italy which observes an annual modulation signature [11]. The Earth's velocity relative to the dark matter distribution changes as the Earth moves around the Sun and produces such a modulation in the dark matter signal rate. This modulation can be observed with terrestrial detectors [12]. The amplitude of the modulation can be positive (i.e. higher rate in June than in December) or negative which depends on WIMP mass and detector threshold. Under certain conditions, it may be possible to observe the 'cross over' point in energy at which the modulation amplitude changes from negative to positive [13].

DAMA/LIBRA claims the evidence for annual modulation with a significance exceeding  $9\sigma$  in 1.33 ton-year of data taken over 14 annual cycles with 100 to 250

kg of NaI(Tl) crystals. Their signal may be caused by light WIMPs, or other types of dark matter producing electrons (see for example [14]) or gamma rays. Those are invisible to direct searches that only extract nuclear recoils. The XMASS detector uses single phase technology and observes only scintillation light by looking for both types of signals. It is able to reach the total DAMA/LIBRA exposure in less than two years with its 832 kg of liquid xenon (LXe). This characteristic of XMASS is particularly important in making this first exploration with a compatible exposure in a different environment and underground site. Moreover, comparing to their energy threshold of 2 keV in electron equivalent ( $\text{keV}_{\text{ee}}$ ), a lower energy threshold of about 1  $\text{keV}_{\text{ee}}$  was achieved in XMASS. This translates directly into higher sensitivity for dark matter searches.

The XMASS detector is located at the Kamioka Observatory (overburden 2700 m.w.e) in Japan. The detailed design and performance are described in [15]. The detector is immersed in a water tank, 10 m in diameter and 10.5 m in height, which is equipped with 72 Hamamatsu H3600 photomultiplier tubes (PMTs), and acts as an active muon veto and a passive radiation shield against neutrons and gamma rays from the surrounding rock. 642 high quantum efficiency (28-40% at 175 nm) Hamamatsu R10789 PMTs are mounted in an approximate sphere with an average radius of 40 cm. The gains of the PMTs were continuously monitored by a blue LED embedded in the inner surface of the detector. Energy calibrations were carried out by regularly inserting a  $^{57}\text{Co}$  micro source [16] into the detector and occasionally also  $^{55}\text{Fe}$ ,  $^{109}\text{Cd}$  and  $^{241}\text{Am}$  sources.

In November 2013, after refurbishing the detector to reduce some of the background sources that were identified in the commissioning run [15], data taking resumed with a significantly improved background situation. The data accumulated between November 2013 and March 2015 were used for this analysis and we selected periods with stable temperature (172.6-173.0 K) and pressure of Xe (0.162 - 0.164 MPa absolute). After removing periods of operation with excessive PMT noise or data acquisition problems, the total live time became 359.2 days.

In this paper, three different energy scales were used: 1)  $\text{keV}_{57\text{Co}}$  denotes an energy scale obtained by dividing the observed photoelectron (PE) by the PE/keV at 122 keV. Therefore  $\text{keV}_{57\text{Co}}$  is proportional to total PE. 2)  $\text{keV}_{\text{ee}}$  represents, an electron equivalent energy incorporating all the gamma-ray calibrations and 3)  $\text{keV}_{\text{nr}}$  denotes the nuclear recoil energy using a factor converting the energy scale from  $\text{keV}_{57\text{Co}}$  to  $\text{keV}_{\text{nr}}$  which was taken from [17]. The 'PE-scaled' energy  $\text{keV}_{57\text{Co}}$  was used throughout the analysis and the final results were translated into  $\text{keV}_{\text{ee}}$  and  $\text{keV}_{\text{nr}}$ . The energy threshold for this analysis is 0.5  $\text{keV}_{57\text{Co}}$  ( $\sim 8$  PE) which corresponds to 1.1  $\text{keV}_{\text{ee}}$  and 4.8  $\text{keV}_{\text{nr}}$ .

Events with equal or more than 4 PMT hits in a 200 ns

coincidence timing window without a muon veto were initially selected resulting in  $3.5 \times 10^7$  events for the energy region between 0.5 and 15  $\text{keV}_{57\text{Co}}$ . In order to avoid events caused by afterpulses of bright events induced by, for example, high energy gamma-rays or alpha particles, we rejected events occurring within 10 ms from the previous event and having a variance in their hit timings of greater than 100 ns (reduce to  $2.9 \times 10^7$  events). A 'Cherenkov cut' removed events which produce light predominantly from Cherenkov emission, in particular from the beta decays of  $^{40}\text{K}$  in the PMT photocathode. Events for which more than 60% of their PMT hits arrive in the first 20 ns were classified as Cherenkov-like events [5] (reduced to  $2.1 \times 10^6$  events). Finally, to remove events that occurred in front of PMTs, we cut on high values of 'Max-PE/Total-PE' where Max-PE and Total-PE are the largest PE counts in one PMT among all PMTs and the total PE in the event, respectively (reduced to  $3.9 \times 10^5$  events). The cut values varied as a function of PE from about 0.2 at 8 PE to about 0.07 at 50 PE. The count rate for the data after the all cuts is 1.9 (0.017) events/day/kg/keV $_{57\text{Co}}$  at 0.5 (5.0)  $\text{keV}_{57\text{Co}}$ .

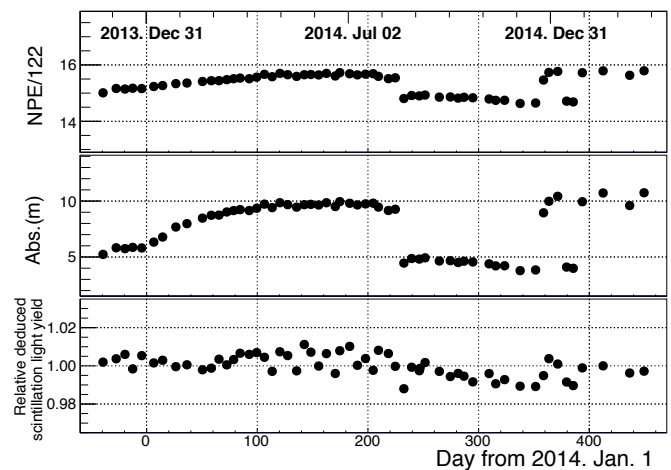


FIG. 1. PE yield monitoring with a  $^{57}\text{Co}$  122 keV gamma ray source. Optical parameters such as absorption length and deduced intrinsic scintillation light yield were obtained by comparing calibration data with MC simulation.

The  $^{57}\text{Co}$  calibration data were taken at various positions along the vertical axis in the detector to track PE yield and optical properties of the LXe. As a variation of about 20% was observed in the position dependence of this PE yield we show the yield appropriately weighted over the entire volume in Fig. 1 (top panel). The PE yield gradually increased after the start of data taking and it encountered a sudden drop due to a power failure in the mine on August 17, 2014. After purification work between December 2014 and January 2015 the highest PE

yield was achieved without recovering the LXe from the detector to a storage tank. Since then the Xe gas evaporating in the detector is continuously circulated through a hot getter and liquefied it at a rate of 1.5 L/min. The absorption and scattering length for the scintillation light as well as intrinsic light yield of the LXe scintillator are extracted from the  $^{57}\text{Co}$  data by using Monte Carlo (MC) simulation [15]. With that we traced the observed PE change in the calibration data as a change in the absorption length, while the scattering length remains stable within  $\pm 0.6\%$  at 52 cm in the standard deviation. We then re-evaluate the absorption length and the relative intrinsic light yield to see the stability of the scintillation light response by fixing the scattering length at 52 cm. The central panel in Fig. 1 traces the absolute absorption length from about 4 m to 11 m and the bottom panel shows the relative change in the intrinsic light yield with its variation staying within  $\pm 0.6\%$  over the entire data taking period.

The time dependence of the PE yield affects the efficiency of the cuts. Therefore we evaluate the absorption length dependence of the relative cut efficiencies through MC simulation. If we normalize the overall efficiency at an absorption length of 8 m, this efficiency changes from  $-4\%$  to  $+20\%$  over the relevant absorption range. The position dependence of the efficiency was taken into account as a correlated systematic error ( $\sim \pm 2.5\%$ ). This is the dominant systematic uncertainty in this analysis. The second largest contribution comes from a gain instability of the FADCs (CAEN V1751) between April 2014 and September 2014 due to a different initialization method used in that period. It contributes  $0.3\%$  uncertainty to energy scale. Other effects from LED calibration, trigger threshold stability, timing calibration were negligible. The observed count rate after cuts as a function of time in the energy region of  $0.5\text{--}1.0\text{ keV}_{^{57}\text{Co}}$  is shown in Fig. 2. The systematic error caused by the relative cut efficiencies are also shown.

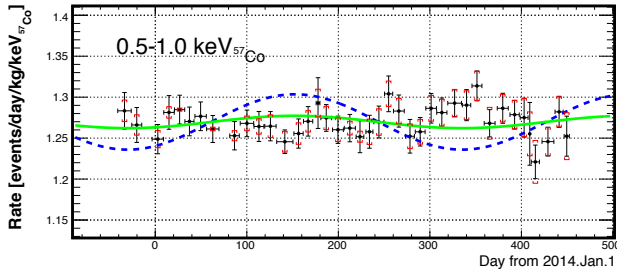


FIG. 2. (color online) Observed count rate as a function of time in the  $0.5 - 1.0\text{ keV}_{^{57}\text{Co}}$  energy range. Errors are statistical only. Square brackets indicate the  $1\sigma$  systematic error for each time bin. The solid and dashed curves indicate the expected count rates assuming 7 and 8  $\text{GeV}/c^2$  WIMPs respectively with a cross section of  $2 \times 10^{-40}\text{ cm}^2$ .

To retrieve the annual modulation amplitude from the data, the least squares method for the time-binned data was used. The dataset was divided into 40 time-bins ( $t_{bins}$ ) with roughly 10 days of live time each. The data in each time-bin were then further divided into energy-bins ( $E_{bins}$ ) with a width of  $0.1\text{ keV}_{^{57}\text{Co}}$ . Two fits were performed independently. Both of them fit all energy- and time-bins simultaneously. Method 1 used a 'pull term'  $\alpha$ , and the method's  $\chi^2$  was defined as:

$$\chi^2 = \sum_i^{E_{bins}} \sum_j^{t_{bins}} \frac{(R_{i,j}^{\text{data}} - R_{i,j}^{\text{ex}} - \alpha K_{i,j})^2}{\sigma(\text{stat})_{i,j}^2 + \sigma(\text{sys})_{i,j}^2} + \alpha^2, \quad (1)$$

where  $R_{i,j}^{\text{data}}$ ,  $R_{i,j}^{\text{ex}}$ ,  $\sigma(\text{stat})_{i,j}$  and  $\sigma(\text{sys})_{i,j}$  are data, expected event rate, statistical and systematic error of the  $i$ -th energy-bin and  $j$ -th time-bin, respectively. The time is denoted as the number of days from January 1, 2014.  $K_{i,j}$  represents the  $1\sigma$  correlated systematic error on the expected event rate based on the relative cut efficiency in that bin. Method 2 used a covariance matrix to propagate the effects of the systematic error. Its  $\chi^2$  was defined as:

$$\chi^2 = \sum_{k,l}^{N_{bins}} (R_k^{\text{data}} - R_k^{\text{ex}})(V_{\text{stat}} + V_{\text{sys}})^{-1}_{kl} (R_l^{\text{data}} - R_l^{\text{ex}}), \quad (2)$$

where  $N_{bins}(= E_{bins} \times t_{bins})$  was the total number of bins and  $R_k^{\text{data(ex)}}$  is the event rate  $R_{i,j}^{\text{data(ex)}}$  for  $k = i \cdot t_{bins} + j$ . The matrix  $V_{\text{stat}}$  contains the statistical uncertainties of the bins, and  $V_{\text{sys}}$  is the covariance matrix of the systematic uncertainties as derived from the relative cut efficiency.

We performed one analysis independent of a specific dark matter model as well as one that assumes WIMP interactions. Hereafter we call the former case as a model independent and the latter case for model dependent analysis. For the model independent case, the expected event rate was estimated as:

$$R_{i,j}^{\text{ex}} = \int_{t_j - \frac{1}{2}\Delta t_j}^{t_j + \frac{1}{2}\Delta t_j} (C_i + A_i \cos 2\pi \frac{(t - t_0)}{T}) dt, \quad (3)$$

where the free parameters  $C_i$  and  $A_i$  were the unmodulated event rate and the modulation amplitude, respectively.  $t_0$  and  $T$  were the phase and period of the modulation, and  $t_j$  and  $\Delta t_j$  was the time-bin's center and width, respectively. In the fitting procedure the modulation period  $T$  was fixed to one year and the phase  $t_0$  to 152.5 days ( $\sim 2\text{nd}$  of June) when the Earth's velocity relative to the dark matter distribution is expected to be maximal. Figure 3 shows these amplitude as a function of energy for both methods after correcting the efficiency. The efficiency was evaluated from gamma ray MC simulation with a flat energy spectrum uniformly distributed in the sensitive volume (Fig. 3 inset). Both methods are in good agreement and find a negative amplitude below  $2\text{ keV}_{^{57}\text{Co}}$ . To evaluate the significance

of this modulation amplitude, we carried out a statistical test by applying the same analysis to 10,000 dummy samples with the same statistical and systematic errors as data but without modulation. The  $\pm 1\sigma$  and  $\pm 2\sigma$  bands in Fig. 3 represent expected amplitude coverage derived from this test applied to method 1. This test gave a  $p$ -value of 6.1% ( $1.9\sigma$ ) for method 1 and of 17% ( $1.4\sigma$ ) for method 2. For both methods the model independent amplitudes they find in the data are consistent with background fluctuations. To be able to test any model of dark matter, we evaluated constraints on the positive and negative amplitude separately in Fig. 3. The upper limit for the amplitudes in each energy bin were calculated by considering only regions of positive or negative amplitude. They were calculated by integrating Gaussian distributions based on the mean and sigma of data ( $=G(a)$ ) from zero. The positive or negative upper limits are satisfied with 0.9 for  $\int_0^{a_{up}} G(a)da / \int_0^\infty G(a)da$  or  $\int_{a_{up}}^0 G(a)da / \int_{-\infty}^0 G(a)da$ , where  $a$  and  $a_{up}$  are the amplitude and its 90% C.L. upper limit, respectively. Method 1 obtained positive (negative) upper limit of  $1.7(-5.1) \times 10^{-2}$  events/day/kg/keV<sub>57Co</sub> between 1.0 and 1.1 keV<sub>57Co</sub> ( $=1.8-1.9$  keV<sub>ee</sub>, or 7.9-8.5 keV<sub>nr</sub>) and the limits get stricter at higher energy. The energy resolution ( $\sigma/E$ ) at 1.0 (5.0) keV<sub>57Co</sub> is estimated to be 36% (18%) comparing gamma ray calibrations and its MC simulation. As a guideline, we make direct comparisons with other experiments not by considering a specific dark matter model but only count rate. The maximum amplitude of  $\sim 2.5 \times 10^{-2}$  events/day/kg/keV<sub>ee</sub> between 2.5 and 3.0 keV<sub>ee</sub> was obtained by DAMA/LIBRA in [11] while XMASS obtains positive upper limit  $1.7 \times 10^{-2}$  events/day/kg/keV<sub>57Co</sub>. Considering that the bin widths in keV<sub>57Co</sub> are wider than in keV<sub>ee</sub> for this energy region, our positive upper limit contradicts their measurement. Note that the energy bin width in Fig. 3 is one fifth of DAMA/LIBRA's so that our limits would even get stricter with DAMA/LIBRA's bin width. Again, it is important to emphasize that the result also covers electron mediated events modulation signature.

In the case of the WIMP dark matter analysis, the expected modulation amplitudes become a function of the WIMP mass  $A_i(m_\chi)$  as the WIMP mass  $m_\chi$  determines the recoil energy spectrum. The expected rate in a bin then becomes:

$$R_{i,j}^{\text{ex}} = \int_{t_j - \frac{1}{2}\Delta t_j}^{t_j + \frac{1}{2}\Delta t_j} \left( C_i + \sigma_{\chi n} \cdot A_i(m_\chi) \cos 2\pi \frac{(t - t_0)}{T} \right) dt, \quad (4)$$

where  $\sigma_{\chi n}$  is the WIMP-nucleon cross section. To obtain the WIMP-nucleon cross section the data was fitted in the energy range of 0.5-15 keV<sub>57Co</sub>. We assume a standard spherical isothermal galactic halo model with the most probable speed of  $v_0=220$  km/s, the Earth's velocity relative to the dark matter distribution of  $v_E = 232 + 15 \sin 2\pi(t - t_0)/T$  km/s, and a galactic escape ve-

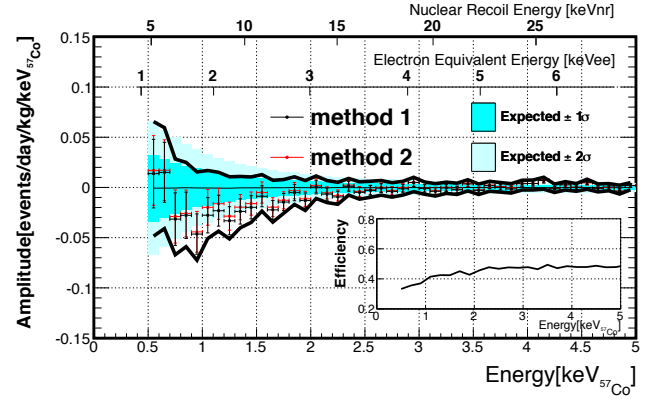


FIG. 3. (color online) Modulation amplitude as a function of energy for the model independent analyses using two methods. Solid lines represent 90% positive (negative) upper limits on the amplitude. The  $\pm 1\sigma$  and  $\pm 2\sigma$  bands represent the expected amplitude region (see detail in the text).

locity of  $v_{esc} = 650$  km/s, a local dark matter density of  $0.3 \text{ GeV}/\text{cm}^3$ , following [13]. In the analysis, the signal efficiencies for each WIMP mass are estimated from MC simulation of uniformly distributed nuclear recoil events in the LXe volume. The systematic error of the efficiencies comes from the uncertainty of LXe scintillation decay time of  $25 \pm 1$  ns [5] and is estimated as about 5% in this analysis. The expected count rate for WIMP masses of 7 and 8  $\text{GeV}/c^2$  with a cross section of  $2 \times 10^{-40} \text{ cm}^2$  for the spin independent case are shown in Fig. 2 as a function of time after all cuts. This demonstrates the high sensitivity of the XMASS detector to modulation. As both methods found no significant signal, the 90% C.L. upper limit by method 1 on the WIMP-nucleon cross section is shown in Fig. 4. The  $-1\sigma$  scintillation efficiency of [17] was used to obtain a conservative limit. The  $\pm 1\sigma$  and  $\pm 2\sigma$  bands in Fig. 4 outline the expected 90% C.L. upper limit band for the no-modulation hypothesis using the dummy samples mentioned above in the model independent analysis. The result excludes the DAMA/LIBRA allowed region as interpreted in [8] for WIMP masses higher than 8  $\text{GeV}/c^2$ . This limit is robust against the difference of analysis methods (less than 10% for the cross section) and astrophysical assumptions (upper limit of  $5.4 \times 10^{-41} \text{ cm}^2$  in the case of  $v_{esc} = 544$  km/s [19]). The best fit parameters in a wider mass range is a cross section of  $3.2 \times 10^{-42} \text{ cm}^2$  for a WIMP mass of 140  $\text{GeV}/c^2$ . This yields a statistical significance of  $2.7\sigma$ , however, in this case, the expected unmodulated event rate exceeds the total observed event rate by a factor of 2, therefore these parameters were deemed unphysical.

In summary, XMASS with its large exposure and high PE yield conducted the annual modulation search to obtain a positive (negative) upper limit amplitude of  $1.7 (-5.1) \times 10^{-2}$  events/day/kg/keV<sub>57Co</sub> between 1.0 and 1.1 keV<sub>57Co</sub> for the model independent anal-

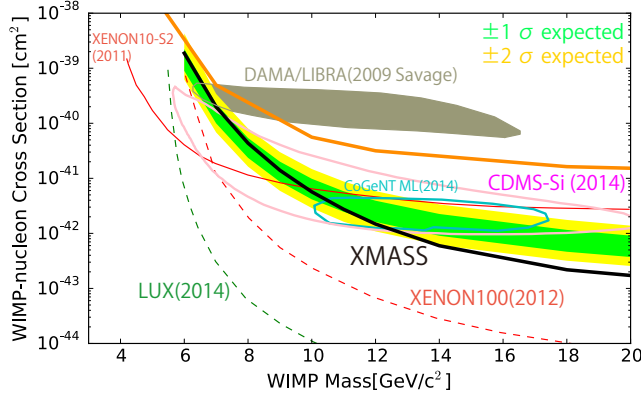


FIG. 4. (color online) Limits on the spin-independent elastic WIMP-nucleon cross section as a function of WIMP mass. The solid line shows the XMASS 90% C.L. exclusion from the annual modulation analysis. The  $\pm 1\sigma$  and  $\pm 2\sigma$  bands represent the expected 90% exclusion distributions. Limits as well as allowed regions from other searches are also shown [2, 3, 5, 8–10, 18].

ysis. As this analysis does not reference only nuclear recoils, simple electron or gamma ray interpretation of the DAMA/LIBRA signal can not be used to evade this limit. For the model dependent analysis, an exclusion upper limit of  $4.3 \times 10^{-41} \text{ cm}^2$  at  $8 \text{ GeV}/c^2$  was obtained and the result excludes the DAMA/LIBRA allowed region for WIMP masses higher than that.

We gratefully acknowledge the cooperation of Kamioka Mining and Smelting Company. This work was supported by the Japanese Ministry of Education, Culture, Sports, Science and Technology, Grant-in-Aid for Scientific Research, JSPS KAKENHI Grant Number, 19GS0204, 26104004, and partially by the National Research Foundation of Korea Grant funded by the Korean

Government (NRF-2011-220-C00006).

- 
- [1] K.A. Olive *et al.*, (Particle Data Group), *Chin. Phys. C*, **38**, 090001 (2014).
  - [2] D.S. Akerib *et al.* (LUX collaboration), *Phys. Rev. Lett.* **112**, 091303 (2014).
  - [3] E. Aprile *et al.* (XENON100 collaboration), *Phys. Rev. Lett.* **109**, 181301 (2012).
  - [4] R. Agnese *et al.* (SuperCDMS collaboration), *Phys. Rev. Lett.* **112**, 241302 (2014).
  - [5] K. Abe *et al.* (XMASS collaboration), *Phys. Lett B* **719**, 78 (2013).
  - [6] K. Abe *et al.* (XMASS collaboration), *Phys. Rev. Lett.* **113**, 121301 (2014).
  - [7] H. Uchida *et al.* (XMASS collaboration), *Phys. Theor. Exp. Phys.*, 063C01 (2014).
  - [8] C. Savage *et al.* *JCAP* **04**, 010 (2009).
  - [9] C. E. Aalseth *et al.* (CoGeNT collaboration), arXiv:1401.6234v1.
  - [10] R. Agnese *et al.* (CDMS collaboration), *Phys. Rev. Lett.* **111**, 251301 (2013).
  - [11] R. Bernabei *et al.*, *Eur. Phys. J. C* **73**, 2648 (2013).
  - [12] A. K. Drukier, K. Freese and D. N. Spergel, *Phys. Rev. D* **33**, 3495 (1986).
  - [13] J.D. Lewin and P.F. Smith, *Astroparticle Phys.* **6**, 87 (1996).
  - [14] E. Aprile *et al.* (XENON100 collaboration) *Phys. Rev. Lett.* **115**, 091302 (2015), E. Aprile *et al.* (XENON100 collaboration) *Science* **349** 6250 851 (2015)
  - [15] K. Abe *et al.* (XMASS collaboration), *Nucl. Instr. Meth. A* **716**, 78 (2013).
  - [16] N. Y. Kim *et al.*, *Nucl. Instr. Meth. A* **784**, 499 (2015).
  - [17] E. Aprile *et al.*, *Phys. Rev. Lett.* **107**, 131302 (2011).
  - [18] J. Angle *et al.* (XENON10 collaboration), *Phys. Rev. Lett.* **110**, 249901 (2013).
  - [19] M.C. Smith *et al.*, *Mon. Not. R. Astron. Soc.* **379**, 755-772 (2007).